IEEE Access
Multidisciplinary | Rapid Review | Open Access Journal

SPECIAL SECTION ON KEY ENABLING TECHNOLOGIES FOR PROSUMER ENERGY MANAGEMENT

Received June 29, 2020, accepted July 15, 2020, date of publication July 22, 2020, date of current version July 31, 2020.

Digital Object Identifier 10.1109/ACCESS.2020.3011170

A Contactless Zero-Value Insulators Detection Method Based on Infrared Images Matching

HONGYING HE[1], (Member, IEEE), ZHUANG HU[1], BOZHONG WANG[2], DIANSHENG LUO[1], (Member, IEEE), WEI-JEN LEE[3], (Fellow, IEEE), AND JINMING LI[4]

[1]College of Electrical and Information Engineering, Hunan University, Changsha 410082, China
[2]State Grid Hunan Electric Power Corporation Maintenance Company, Changsha 410004, China
[3]Energy Systems Research Center, The University of Texas at Arlington, Arlington, TX 76019, USA
[4]State Grid Hunan Electric Power Corporation Economic and Technical Research Institute, Changsha 410004, China

Corresponding authors: Hongying He (lhx20070322@sina.com) and Zhuang Hu (1913221010@qq.com)

This work was supported in part by the National Natural Science Foundation of China under Grant 51722701, in part by the National Key Research and Development Plan, China, in 2017, under Grant 2017YFB0903403, and in part by the Natural Science Foundation of Hunan Province, China, in 2019, under Grant 2019JJ40019.

ABSTRACT A contactless method based on infrared image matching is presented for zero-value insulator detection on outdoor porcelain insulator string. An improved SIFT (scale-invariant feature transformation) method is developed to extract features and accomplish the pre-matching between the insulator string to be detected and the standard string in the image library. An improved RANSAC (random sampling consistency) algorithm is developed to remove mismatching points and achieve more accurate and faster detection. Firstly, an adaptive circle window is designed to improve the sensitivity of the SIFT operator on arc features extraction from insulators. Then, the dimension of the feature is decreased from128 to 32 by dividing the circle into 4 fan-shaped regions and descript the feature on 8 directions to achieve the lower computation burden and high accuracy. For the SIFT method and RANSAC method uses Euclidean distance to measure the similarity between features extracted from the string to be detected and the string in the standard library, mismatching may be caused. Spatial geometric features of the neighborhood around the feature point are used to construct the error function to improve the RANSAC method and remove the mismatching points. Faster matching is obtained by a threshold control for decreasing the number of data checking for the consensus set data models. Testing results show that the presented method is effective in the detection of zero-value resistances for outdoor insulator string. Compare with the SIFT method and SIFT + RANSAC method, the presented method has higher accuracy and faster detection speed.

INDEX TERMS Zero-value insulator detection, infrared imaging, image matching, adaptive circle template, spatial geometric features, prosumer infrastructure.

I. INTRODUCTION

Outdoor insulators are exposed in the air, suffered from rain, snow, frost, dew, etc., endures long-term operating voltage and wire tension, which may result in insulation failure. Under severe cases, they may cause zero-value insulators and leads to single-phase grounding, flashover, breakdown, or power outage. This will seriously affect the safe operation of the power grid and introduce significant financial losses.

As an issue that may impact the safe operation of the grid, the detection of zero-value insulators has drawn worldwide concern. Voltage distribution method [1], corona pulsed method [2], electric field distribution method [3], surface flashover voltage method [4], [5], and UHF method [6] are commonly used among the industry. Traditional methods are limited by tower detection, vulnerable to electromagnetic interference, or require power interruption. Some new methods are developed by using optics, acoustics, image processing, and artificial intelligence technology. A sensitive insulator life detection method is proposed in [7]. Sound wave and the ultrasonic wave is applied on faulty insulators detection of high-voltage transmission line in [8]–[11]. In recent years, aerial photos and image processing technology are also involved in failure insulator online detection [12]. As a

The associate editor coordinating the review of this manuscript and approving it for publication was Huai-Zhi Wang.

non-intrusive method, the infrared imaging method has advantages on visualization, safety, non-contact, immune to electromagnetic interference, and convenience for live detection. Several successful applications have been reported on fault diagnosis of power equipment with an unusual temperature rise [13], [14].

Normally, porcelain insulators have resistance value more than 300MΩ, but insulators whose resistance value less than 5 MΩ are regarded as zero-value insulators. Compare with the normal insulators, zero-value insulators have lower temperatures with less heat emission. Thus, they have distinct image features. Zero-value insulators occupy a lower gray rang and normal insulators occupy the higher rang. Based upon this feature, an image matching method combined with the scale-invariant feature transformation (SIFT) method [15] and the Random sampling consistency algorithm (RANSAC) method [16] is presented in this paper for zero-value insulators detection. SIFT method is used for pre-matching the zero-value insulator string to be detected with the standard string in the image library and the RANSAC method is used to achieve further matching and remove the mismatching points. Aiming to achieve high accuracy and fast detection, improvements both on the SIFT method and the RANSAC method are developed in this paper.

SIFT algorithm performs well on scaling, translation, and rotation invariability. It is widely used on feature extraction and image matching. However, the SIFT operator extracts the features on 8 directions in a 4*4 square window and using a 128-dimension vector to descript the features. The shapes of the contour of insulator image are ellipse and the outline are made of arcs, but the square window is insensitive on arc detection, which may result in mismatching. Besides this, high dimensional feature vectors may cause feature redundancy and high computation costs. In this paper, an improved SIFT operator using an adaptive circle window is designed to achieve high sensitivity for arc features detection of insulators. Then, the dimension of the feature is decreased from 128 to 32 by dividing the circle into 4 fan-shaped regions and descript the feature on 8 directions to achieve lower computation burden and high accuracy.

As a normal procedure, Euclidean distance is used in the SIFT method to accomplish image matching after feature extraction. However, the SIFT algorithm just simply uses the Euclidean distance ratio between the feature point's nearest neighbor distance and the second nearest distance to make matching. Therefore, when a similar feature appears, mismatching often occurs for neglecting the location, the structure, and the order of the feature vectors in the space. In this paper, an improved RANSAC method is used to remove the mismatching points. Geometry space characteristics constructed by the feature point and six points in its neighborhood are proposed to further enhance the accuracy of the RANSAC method. At the same time, time consumption is decreased by setting a threshold for the data numbers used to check the correctness of the data consensus setting models. Experiment results show high accuracy and fast matching between zero-value insulator strings and the standard insulator strings is achieved by the implementation of the presented method.

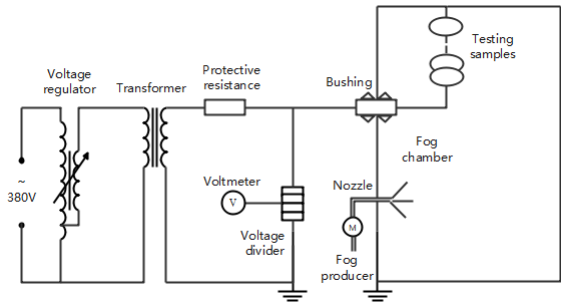

FIGURE 1. Test circuit diagram.

II. TEST SETUP AND IMAGE ACQUISITION

The test was set up in a 4.0m * 4.0m * 4.0m artificial fog chamber. 210 pieces of XP-160 porcelain suspension insulator were taken as the test insulator string. Images have been taken by infrared camera FLIR S65 through a glass window on the chamber. The circuit diagram of the testing is shown in Figure 1. To simulate the outdoor 110 kV (line voltage) operation situation, a shifting coil voltage regulator (KZX-51022) and a test transformer (JZ/YD) are used to lower the voltage. Then, 63.5 kV phase voltage is generated by a capacitive voltage divider (SGB-200A) and sent to the fog chamber through a 110-kV wall bushing.

The humidity range of the circumstances is adjusted from 78% to 92% by a fog producer [17]. 210 insulators were divided into 30 groups, with each group having 7 insulators in series. Among them, 6 of them are normal insulators (resistance value of each one more than 500 MΩ), one of them is a zero-value insulator (resistance value less than 5 MΩ). To simulate the outdoor situation, the pollution levels of the insulator are artificially contaminated from level 0 to level 3 (Contaminated according to IEC60507) [18]. 1800 images for zero-value insulator strings were obtained by the infrared camera. 1450 images are used to build the criterion image library (covers all images with zero- value insulator at different positions on the string) and the rest 350 images are used as testing samples.

For infrared images of insulators that have high noise and low contrast, a wavelet denoising method based on Wavelet and MAP estimation [19] is used to depress the noise and improved the quality of the image. Then, the improved SIFT method presented is used to extract the insulator string features and pre-match the string with the ones in the zero-resistance insulator image library. Lastly, mismatching points are removed by the improved RANSAC method presented here and achieve high accuracy.

III. FEATURE EXTRACTION AND PRE-MATCHING BASED ON IMPROVED SIFT METHOD

A. FEATURE EXTRACTION

Since the heat state of zero-value insulators differs distinctly with normal insulators, they have different gray rang and

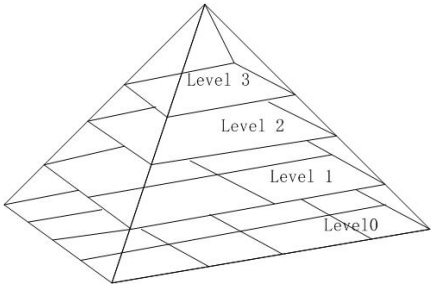

FIGURE 2. Gaussian pyramid.

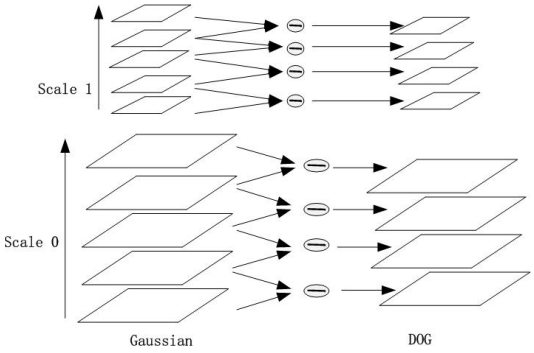

FIGURE 3. DOG image.

different features in infrared images. The identification of zero-value insulator is theoretically feasible due to the difference of insulator gray distribution. But images matching between the string to be detected and the one in the image library may be challenged by suspension height, shooting distance, shooting angel. Thus, the feature extraction method is critical for subsequent accurate identification. In this paper, the SIFT method [20] is applied to feature extraction for its advantages on rotation, translation, and scale invariance. First, to obtain detailed features of the insulator string, the Gaussian kernel function is used to construct multi-scale space. Then, the convolution operation is applied to accomplish linear translation invariance. Last, the difference operator is used to extract the image features of the zero-value insulator string. Gaussian difference function and Gaussian kernel function is shown in (1) and (2).

$$D(x, y, \sigma) = I(x, y) * (G(x, y, k\sigma) - G(x, y, \sigma)) \quad (1)$$

$$G(x, y, \sigma) = \frac{1}{2\pi\sigma^2} \exp(-\frac{x^2 + y^2}{2\sigma^2}) \quad (2)$$

where σ is the scale control factor. The original image is convolved with the Gaussian kernel function and the Gaussian pyramid image is formed by continuous down-sampling on different scales (shown in Figure 2).

As shown in (1) and Figure 2, the difference of Gaussian (DOG) operators are used to obtain Gaussian difference images (shown in Figure 3) by Gaussian filtering and subtraction operation, where k is the filter template control coefficient.

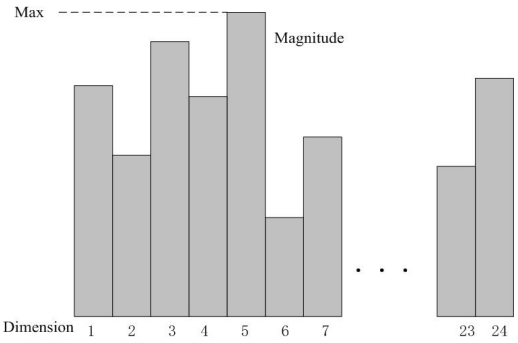

FIGURE 4. Gradient histogram in 24 directions.

Then, features are obtained by slide a 3*3 square window to compare the central point with the 26 points in its' neighborhood and the corresponding area in upper and lower levels.

B. FEATURE DESCRIPTION

After obtaining all feature points on different scales, the direction parameters of each feature point are calculated. SIFT algorithm aligns coordinates with the main direction of the feature to achieve rotation invariance. The main direction of the feature is obtained by statist histogram peak of the feature gradient in the featured neighborhood. The direction with the largest histogram peak is the main direction of the feature. The description of features is in a 16*16 square neighborhood around the feature point and the neighborhood is divided into 16 squares. In each square, Gaussian weighted are performed to calculate the gradient of the feature on 8 directions. Thus, 128-dimensional vectors are obtained for one feature point description. The algorithm uses 128-dimensional vectors to describe one feature point, which results in information redundancy and computing overhead.

C. IMPROVEMENT OF FEATURE EXTRACTION AND DESCRIPTION

SIFT algorithm use square templates to calculate gradient information in the neighborhood, which has a good effect on detecting corner points. But the zero-value insulator image has high noise and low contrast, and the contour line of the insulator is a circular arc. The square template is insensitive for arc detection of insulators; therefore, a circular template is more suitable for feature extraction and description. Since the feature extraction is based on the processing of Gaussian convolution, the distribution characteristics of the Gaussian function determine that the points outside 3σ contribute little to the feature description. An adaptive circle template with the 3σ length radius is designed in this paper for the feature calculation and description. The gradient histogram is calculated on 24 directions for the feature (per 15 degrees for a direction). The gradient histogram on 24 directions is Shown in Figure 4.

The circle template is divided into four fan-shaped areas. Gaussian weighted is applied to complete the gradient histogram accumulation in each area. Histograms whose peak

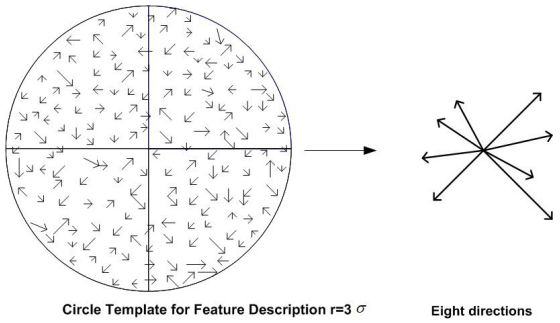

FIGURE 5. Feature description operator.

before 8 in 24 directions are picked out for feature description, Therefore, the dimension of the feature description vector is reduced to 4 * 8 = 32 (shown in Figure 5), which greatly reduces the calculation consumption and improves the matching speed. Meanwhile, the reduction of the dimension of the feature vector avoids the excessive feature selection and depress the mismatching rate.

D. IMAGE PRE-MATCHING OF ZERO-RESISTANCE INSULATOR STRINGS

The matching of image features depends on the similarity between features of the original image and the target. SIFT algorithm adopts Euclidean distance to match the image. A feature point pairs pre-matching is determined by setting the threshold of Euclidean distance proportion between the nearest and the second nearest point in the candidate feature sets. In this paper, the threshold is set to 0.8 to matching the original zero-insulator string images and the string in the library.

Since Euclidean distance just equally treats each vector in the feature, other attributes of the feature such as spatial position and geometric space constraints are not concerned, which often results in mismatching. Therefore, the RANSAC algorithm is often used to purify feature matching.

IV. MISMATCHING POINTS REMOVED BY IMPROVED RANSAC METHOD

A. RANSAC METHOD

RANSAC algorithm uses the best consensus set to achieve matching. It constructs the data model by randomly extracting data from the pre-matched feature set, obtain the best model in an iterative way, and remove the mismatching points through the threshold setting of the error function. Steps of the method are as follows:

1) 4 pairs of features are randomly selected from the original set and the candidate set to calculate the homography matrix H between the original image and the matching image.

2) Calculate the rest n-4 features' mapping results through the matrix H, and Euclidean distance is used as an error function to measure the similarity between the feature points obtained by H matrix transformation and the candidate features.

3) If the Euclidean distance is less than ε, the candidate feature point is considered as a right point fits the data model, and matrix H is renewed with the newly joined points. otherwise, it will be discarded as the 'outer' point unable fits the model.

4) Repeat the process above through all the data, the data model with the maximum number of points is regarded as the best consensus set model.

Though the RANSAC method has efficiency on mismatching points removing, it may still have problems with accuracy in case of infrared images with high noise and low contrast. Besides, it is time-consuming for a large number of iterations, especially when the 'outer' points are excessive.

B. IMPROVEMENT OF RANSAC METHOD ON ACCURACY

To overcome the shortcomings of Euclidean distance's treating the vectors of the feature equally, an error function is constructed based on spatial geometric features of the neighborhood around the feature points to further improve the accuracy of RANSAC method. The geometric spatial structure composed of the feature points and the six nearest points in the neighborhood is shown in below.

Taking the feature point (x, y) as the center of a neighborhood, the geometry distance $d_1, d_2, \cdots d_6$ between the center and the nearest six points $(x_1, y_1), (x_2, y_2) \cdots (x_6, y_6)$ in the neighborhood are calculated as,

$$d_i = \left((x - x_i)^2 + (x - y_i)^2\right)^{1/2} \tag{3}$$

In order to make the feature have the invariance on scaling, the distance proportional coefficient $(r_1, r_2, \cdots r_6)$ is constructed as follows,

$$r_i = \frac{d_i}{d_1 + d_2 + d_3 + d_4 + d_5 + d_6} \tag{4}$$

Starting from the shortest distance, the angles $\theta_1, \theta_2, \cdots \theta_6$ between vectors are calculated follows the counter-clockwise direction.

When $0 \le \theta_i \le \frac{\pi}{2}$,

$$\theta_i = \arccos\left(\frac{d^2_{AA_i} + d^2_{AA_{i+1}} - d^2_{A_iA_{i+1}}}{2d_{AA_i}d_{AA_{i+1}}}\right) \tag{5}$$

When $\frac{\pi}{2} \le \theta_i \le \pi$,

$$\theta_i = \pi - \arccos\left(\frac{d^2_{AA_i} + d^2_{AA_{i+1}} - d^2_{A_iA_{i+1}}}{2d_{AA_i}d_{AA_{i+1}}}\right) \tag{6}$$

Since the value of r_i is on the range of (0,1), the angle θ_i is also normalized to (0,1)by (7),

$$\alpha_i = \frac{\theta_i}{180} \tag{7}$$

Geometry feature vector constructed by spatial distance $r = (r_1, \cdots, r_6)$ and angle information $\alpha = (\alpha_1, \cdots, \alpha_6)$ is as,

$$v_i = w_i r_i + \omega_i \alpha_i \tag{8}$$

where w_i and ω_i are the weight coefficient of r_i and α_i, respectively. Then, the error function is designed as,

$$E_j = \exp \sum_{j=1}^{6} \frac{|v_{jA} - v_{jB}|}{|(v_{jA} + v_{jB})/2|} - 1 \tag{9}$$

where v_{jA} and v_{jB} corresponding to the jth geometric feature vector comes from the original image A and the image B to be matched in the library. Setting the threshold of the error function E_j, choose those points whose error less than ε as the 'inner' point which fits the data model.

C. IMPROVEMENT OF RANSAC METHOD ON TIME CONSUMPTION

Time consumption T of the whole matching process can be divided into two parts, the time for pre-matching T_1 and the time for precise matching T_2 by the RANSAC method. Namely,

$$T = T_1 + T_2 \tag{10}$$

T_1 is greatly decreased by replacing 128-dimensional vectors with 32-dimensional vectors for feature description. Originally, T_2 is combined by two parts, the first part is data model construction time, including data sampling time and time on H matrix parameters calculation. For homograph transform needs 4 pairs of points to construct each data model and determine the H matrix. Time costs on the data model is $C_n^4 T_{se}$, and data checking should be applied to each data model, thus, the time costs on the rest $(n-4)$ points for the C_n^4 data model is $C_n^4(n-4)T_t$.

$$T_2 = C_n^4 T_{se} + C_n^4(n-4)T_t \tag{11}$$

where n is the number of the feature points, T_{se} is time costs on build each data model. T_t is the time consumption for checking each datum on each data model.

For RANSAC method needs the construct data model for every 4 points pairs, and model checking is applied through all data, the time costs is huge. Aiming at fast matching, improvement is developed from two aspects in this paper,

First, the affine transform is used to substitute the homography transform. For the affine matrix can be determined with only 3 pairs of feature points, the number of data sampling is decreased from C_n^4 to C_n^3. Based on this, time costs on data checking and model checking are decreased.

Then, the threshold is set for numbers of data applied to data model correctness checking. For RANSAC method is just applied on data that have been pre-matched by SIFT to make more precise matching and the right data model should fit most of the data. In this paper, data models whose outer points numbers more than 3% of the inner points are discarded as fake data models and data checking will be terminated at the same time.

Thus, time costs T_2 is largely reduced to T_2' by performing the two ways above to attain fast image matching.

$$T_2' = C_n^3 T_{se} + C_n^3 N_t T_t \tag{12}$$

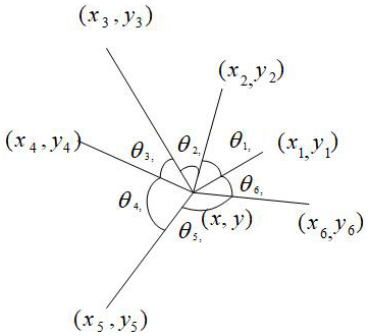

FIGURE 6. Spatial geometric construction of the feature point with its' neighborhood.

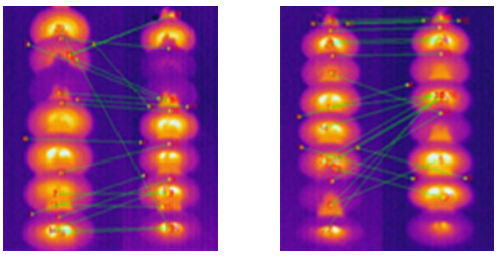

FIGURE 7. Matching results by sift method.

where N_t is the number of the data applied to each data model which controlled by the threshold.

V. IMAGE MATCHING RESULTS AND ANALYSE

A. INFLUENCE OF LOCATION ON THE STRING

Figure 7 are matching results with the SIFT algorithm. (in all images from Figure 7(a) to Figure 11(d), images on left is the string to be detected, images on right is matching images comes from the image library). In Figure 7(a), the third piece near the high voltage end is the zero -value insulator. But the image on the right of Figure 7(a) shows a mismatching result with two pieces of zero-value insulators on the matched string.). Like Figure 7(a), Figure 7(b) also shows another mismatching result. In the left image, the second piece near the ground end is the zero-value insulator, but the matched string has the zero-insulator on the fourth piece. We can see from matching results that the SIFT algorithm makes some serious mismatching on the detection of zero-value insulators string. The reason is partly for that the SIFT algorithm uses the square window to extract features, which is insensitivity on arc features extracting. The other reason is on its' feature matching use Euclidean distance to measure. Euclidean distance matching treats all components of the feature vector equally, yet, the difference between feature attributes have not been considered.

In this paper, a circular feature calculation template is proposed to improve the sensitivity of arc features detection. The geometric properties of the neighborhood space around the feature points were combined with the RANSAC algorithm to perform further delicate matching and remove

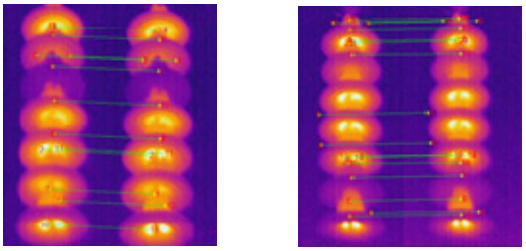

(a) (b)

FIGURE 8. Matching results by improved RANSAC method.

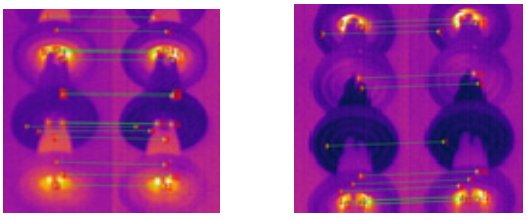

(a) (b)

FIGURE 9. Matching results on different contamination levels.

the mismatching points. Figure 8(a) and Figure 8 (b) are matching results for the same string in Figure 7 processed by the presented method. Compared to the view of Figure 7 and Figure 8, despite their location, the zero-value insulator string is accurately matched with the right strings in the library. (Note that contamination severity is on level 3). It indicates the proposed method has high accuracy on zero-value insulator detection.

B. INFLUENCE OF CONTAMINATION

Figure 9 shows the matching results of zero-value insulator images taken by the wide-angle lens at different contamination levels. Figure 9(a) shows the matching results of the zero-value insulator string at contamination level 2, and Figure 9(b) shows the matching results of zero-value insulators at contamination level 1.

We can see from the figure, though the contamination level seriously affects the heat state of the normal insulator surface, it hardly affects the thermal state of zero-value insulators. In the images, the area of normal insulator looks far brighter than zero-value insulators. Compared Figure 9(a) (contamination level 2) and Figure 9(b) (contamination level 1), we can find that the greater the level is, the more heat the normal insulator emit. Though normal insulators' heat emission in Figure 9(b) is lower than that in Figure 9(a), normal insulator and zero-value insulator's heat state is still distinctly different. The method proposed in this paper still achieves high identification accuracy for zero-value insulators. The presented method is applicable for zero-value insulator detection on different pollution levels.

C. INFLUENCE OF SUSPENSION HEIGHT, SHOOT-ING DISTANCE AND SHOOTING ANGLE

The matching accuracy of zero-value insulator image may also be affected by such factors as suspension height, shooting distance, shooting Angle, etc.

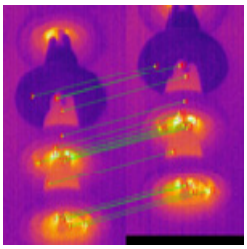

FIGURE 10. Matching results on different suspension height.

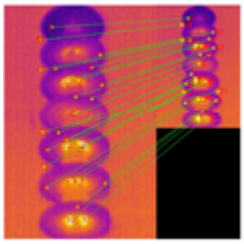

FIGURE 11. Matching results on different shooting distance.

Figure 10 shows the matching result of two insulator strings both with the zero-value insulator on the third piece near the ground end but hung at a different height. We can see from the view of image matching results that accurate matching still having been attained through strings is hung vertically at a different height. It indicates suspension height hardly affect the detection accuracy. The reason lies in that the presented method using Laplace differential operator and convolution operation to extract features and achieve excellent translation invariance. It shows the presented method has good adaptability when the suspension height of insulators differs.

Figure. 11 (with the zero-value insulator on the first piece at high voltage end) shows the matching results of zero-value insulator strings taken at the different shooting distances (the shooting distance of the image on left is 3 meters and the right one is 5 meters). It can be seen that though the images have different size by shoot at a different distance, accurate matching is still available by using Laplace pyramid to extract features which achieves invariance on different scales. It indicates the presented method has good performance when shooting distance changes.

Figure12 (a)-12 (d) are matching results of the same insulator string corresponding to a rotation angle of 45 degrees, 90 degrees, and 135 degrees. Though the image is rotated at various angles, good rotation invariance is still obtained in the proposed method by using a designed circular window for the feature extraction and a specification main direction for the feature. We can see from Figure 12 (a) to Figure 12 (d), the zero-insulator string is well-matched with the zero-value insulator strings in the library. It indicates that the proposed method has high detection accuracy and is hardly interfered with by shooting angle.

VI. ACCURACY COMPARISON OF DIFFERENT METHODS

In order to compare the accuracy of different methods, SIFT, SIFT + RANSAC, and the method proposed in this paper

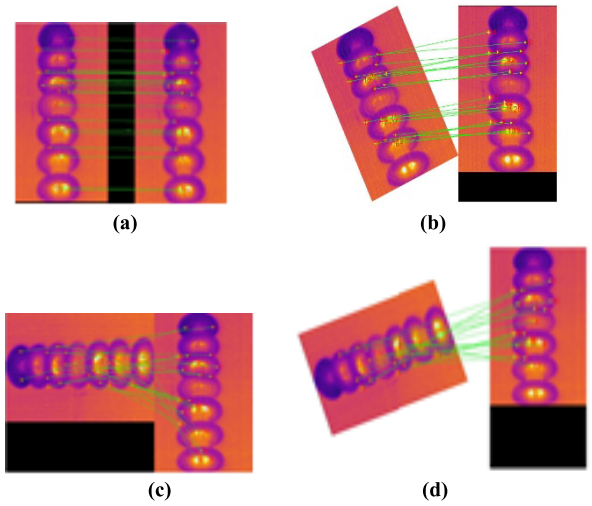

FIGURE 12. Matching results on different shooting angles.

TABLE 1. Accuracy comparison of the methods.

Method	N_1	N_2	P
SIFT	9065	1328	85.35%
SIFT+RANSAC	8248	889	89.22%
Presented method	7323	251	96.57%

were performed to match 350 zero-value insulator string images with the standard zero-value insulator string images in the image library. The results are shown in Table 1. We can see from Table.1 that, although the SIFT method obtained many feature point pairs, it contained many wrong feature points, the accuracy is just 85.35%. SIFT + RANSAC method performed further matching on the basis of pre-matching by SIFT. It removed some mismatching pairs and enhanced the accuracy to 89.22%. But the accuracy still needs to improve. The method proposed in this paper reduces the occurrence of fake features and improves the matching accuracy by using a circular template that is designed for feature extraction for insulator arc contour. Matching accuracy is further improved by 96.57%. It is contributed to the error function which is constructed by the geometric spatial information of the feature.

VII. COMPARISON OF TIME COSTS OF DIFFERENT METHODS

Table 2 shows the time consumption on image matching by the SIFT method, SIFT + RANSAC method, and the method presented in this paper for 350 insulator images to be measured. From the results in Table 2, We can draw conclusions as following, the SIFT algorithm uses 128-dimensional vectors to describe features, which occupies lots of storage space and the computational burden is high. Though the accuracy of SIFT + RANSAC method is higher than SIFT (shown in Table 1), but time consumption is largest among the three, for its' matching based on the pre-matching results of SIFT and using iteration method to acquire the best consensus set as well as the data model test should go through all over the data. As shown in Table 2, the presented method is far superior to the other two on time consumption. The reason lies in following, first, using the 32-dimensional vector describes the feature, effectively reduce the feature storage and computing time. Then, not like the RANSAC method uses iteration and testing data model go through all data, the presented method uses a threshold to limit the number of the data on the model correctness test.

TABLE 2. Time consumption of different methods.

	SIFT	SIFT+RANSC	Presented method
N_1	9065	8248	7623
t (s)	66.53	76.21	47.75

VIII. CONCLUSION

An improved SIFT algorithm combined with an improved RANSAC method is proposed in this paper for zero-value insulator detection. A circular window is designed to overcome the shortage of insensitivity of the square window on arc feature extraction of insulators. geometry space feature involved 6 points in the feature point neighborhood is used to construct error function and achieve higher accuracy. Computation consumption costs are lowed by using 32 dimension-feature substitutes 128 dimension-feature. A threshold is setting for cutting down the time expense on data model correctness checking. Testing results and analysis shows that compared with the SIFT method, SFT + RANSAC method, the presented method achieves higher accuracy and faster detection and hardly affected by zero-value insulator location, contamination levels, detection distance, shooting angle, and suspension height. It provides a contactless, safe, economic way for zero-value insulators detection and hardly affected by electromagnetic interference.

REFERENCES

[1] Z. Jiang, W. Wu, B. Wang, P. Xie, H. Li, and F. Lin, "Design and test of 500-kV lightning protection insulator," *IEEE Access*, vol. 7, pp. 135957–135963, 2019.

[2] Y. Kim and K. Shong, "The characteristics of UV strength according to corona discharge from polymer insulators using a UV sensor and optic lens," *IEEE Trans. Power Del.*, vol. 26, no. 3, pp. 1579–1584, Jul. 2011.

[3] G. H. Vaillancourt, S. Carignan, and C. Jean, "Experience with the detection of faulty composite insulators on high-voltage power lines by the electric field measurement method," *IEEE Trans. Power Del.*, vol. 13, no. 2, pp. 661–666, Apr. 1998.

[4] U. K. Kalla, R. Suthar, K. Sharma, B. Singh, and J. Ghotia, "Power quality investigation in ceramic insulator," *IEEE Trans. Ind. Appl.*, vol. 54, no. 1, pp. 121–134, Jan. 2018.

[5] M. M. Hussain, S. Farokhi, S. G. Mcmeekin, and M. Farzaneh, "Mechanism of saline deposition and surface flashover on outdoor insulators near coastal areas part II: Impact of various environment stresses," *IEEE Trans. Dielectr. Electr. Insul.*, vol. 24, no. 2, pp. 1068–1076, Apr. 2017.

[6] K. L. Wong, "Application of very-high-frequency (VHP) method to ceramic insulators," *IEEE Trans. Dielectr. Electr. Insul.*, vol. 11, no. 6, pp. 1057–1064, Dec. 2004.

[7] X. Shen, X. Jiang, Y. Cheng, and M. MacAlpine, "A novel method for live detection of faulty direct current insulators," *IEEE Trans. Power Del.*, vol. 23, no. 1, pp. 24–30, Jan. 2008.

[8] H. Ha, S. Han, and J. Lee, "Fault detection on transmission lines using a microphone array and an infrared thermal imaging camera," *IEEE Trans. Instrum. Meas.*, vol. 61, no. 1, pp. 267–275, Jan. 2012.

[9] K.-C. Park, Y. Motai, and J. R. Yoon, "Acoustic fault detection technique for high-power insulators," *IEEE Trans. Ind. Electron.*, vol. 64, no. 12, pp. 9699–9708, Dec. 2017.

[10] Z. Hu, T. He, Y. Zeng, X. Luo, J. Wang, S. Huang, J. Liang, Q. Sun, H. Xu, and B. Lin, "Fast image recognition of transmission tower based on big data," *Protection Control Mod. Power Syst.*, vol. 3, no. 1, pp. 149–158, Dec. 2018.

[11] P. Gopakumar, B. Mallikajuna, M. Jaya Bharata Reddy, and D. K. Mohanta, "Remote monitoring system for real time detection and classification of transmission line faults in a power grid using PMU measurements," *Protection Control Mod. Power Syst.*, vol. 3, no. 1, pp. 159–168, Dec. 2018.

[12] D. Pernebayeva, A. Irmanova, D. Sadykova, M. Bagheri, and A. James, "High voltage outdoor insulator surface condition evaluation using aerial insulator images," *High Voltage*, vol. 4, no. 3, pp. 178–185, Sep. 2019.

[13] H. He, W. Lee, D. Luo, Y. Cao, Z. Zhan, and T. Lu, "A contactless insulator contamination levels detecting method based on infrared images features and RBFNN," *IEEE Trans. Ind. Appl.*, vol. 55, no. 3, pp. 2455–2463, May/Jun. 2019.

[14] D. Lopez-Pérez and J. Antonino-Daviu, "Application of infrared thermography to failure detection in industrial induction motors: Case stories," *IEEE Trans. Ind. Appl.*, vol. 53, no. 3, pp. 1901–1908, May 2017.

[15] D. G. Lowe, "Distinctive image features from scale-invariant key points," *Int. J. Comput. Vis.*, vol. 60, no. 2, pp. 91–110, Nov. 2004.

[16] D. Morley and H. Foroosh, "Improving RANSAC-based segmentation through CNN encapsulation," *IEEE Signal Process. Lett.*, vol. 27, no. 10, pp. 757–761, 2016.

[17] R. J. C. Wood, "Spray and fog tests on 220-Kv. Insulators," *Trans. Amer. Inst. Electr. Eng.*, vol. 49, no. 1, pp. 9–13, Jan. 1930.

[18] *Artificial Pollution Tests on High-Voltage Ceramic and Glass Insulators to Be Used on A.C. System*, IEC Standard 60507, IEC International Standard, 2013.

[19] H. He, W.-J. Lee, D. Luo, and Y. Cao, "Insulator infrared image denoising method based on wavelet generic Gaussian distribution and MAP estimation," *IEEE Trans. Ind. Appl.*, vol. 53, no. 4, pp. 3279–3284, Jul. 2017.

[20] F. Dellinger, J. Delon, Y. Gousseau, J. Michel, and F. Tupin, "SAR-SIFT: A SIFT-like algorithm for SAR images," *IEEE Trans. Geosci. Remote Sens.*, vol. 53, no. 1, pp. 453–466, Jan. 2015.

HONGYING HE (Member, IEEE) received the B.S. degree in electronics engineering from Jilin University, Changchun, China, in 1998, and the Ph.D. degree in electrical engineering from Hunan University, Changsha, China, in 2006. She joined Hunan University, in 2007, where she is currently an Associate Professor with the College of Electrical and Information Engineering. Her fields of interests mainly include high-voltage insulation detection, electric power equipment fault identification, load forecasting, image processing, and artificial intelligence. She is a member of the IAS.

ZHUANG HU received the B.S. degree in electrical engineering from the Hefei University of Technology, Hefei, China, in 2019. He is currently pursuing the M.S. degree with the College of Electrical and Information Engineering, Hunan University, Changsha, China. His major research interests include power system planning and operation.

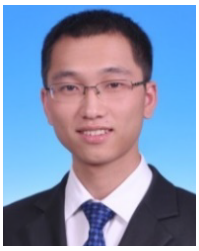

BOZHONG WANG received the B.S. and M.S. degrees in electrical engineering from North China Electric Power University, Beijing, China, in 2009 and 2012, respectively. He is currently a Power Grid Engineer with State Grid Hunan Electric Power Corporation Maintenance Company, Changsha, China. His major research interests include power system operation, reliability, and maintenance.

DIANSHENG LUO (Member, IEEE) was born in Hunan, China, in 1971. He received the B.S., M.S., and Ph.D. degrees from Jilin University, Changchun, China, in 1994, 1997, and 2000, respectively, all in power engineering. He joined Hunan University, in 2001, where he is currently a Professor with the College of Electrical and Information Engineering. His research mainly focuses on the outdoor insulation online detection of power equipment, image processing, load forecasting, smart grid, renewable energy, power quality, demand-side management, and smart home.

WEI-JEN LEE (Fellow, IEEE) received the B.S. and M.S. degrees from National Taiwan University, Taipei, Taiwan, in 1978 and 1980, respectively, and the Ph.D. degree from The University of Texas at Arlington, Arlington, in 1985, all in electrical engineering. He is currently a Professor with the Department of Electrical Engineering and the Director of the Energy Systems Research Center, The University of Texas at Arlington. Since 2008, he has been served as the Project Manager of the IEEE/NFPA Arc Flash Research Project. He has been involved in research on arc flash and electrical safety, utility deregulation, renewable energy, smart grid, microgrid, load forecasting, power quality, distribution automation and demand-side management, power systems analysis, online real-time equipment diagnostic and prognostic systems, and microcomputer-based instrumentation for power systems monitoring, measurement, control, and protection. He is a registered Professional Engineer in the state of Texas.

JINMING LI received the B.S. and M.S. degrees in electrical engineering from the South China University of Technology, Guangzhou, China, in 2011 and 2014, respectively. He is currently a Power Grid Engineer with State Grid Hunan Electric Power Corporation Economic and Technical Research Institute, Changsha, China. His major research interests include power system planning and reliability.